Electronic Supplementary Material (ESI) for Physical Chemistry Chemical Physics.
This journal is © the Owner Societies 2019

Supporting information

Title: **Strongly resonant metasurfaces supported by reflective substrates for highly efficient second- and high-harmonic generations with ultralow pump intensity**

Kwang-Hyon Kim[1,*] *and Wi-Song Rim*[1,2]

[1]Institute of Physics, State Academy of Sciences, Unjong District, Pyongyang, Democratic People's Republic of Korea

[2]Institute of Lasers, State Academy of Sciences, Unjong District, Pyongyang, Democratic People's Republic of Korea

* E-mail: kwang-h.kim@star-co.net.kp.

S1. Intensity enhancement and reflectance depending on the structural parameters of the metasurface

The electromagnetic responses of the metasurfaces composed of plasmonic nanoantenna arrays have been evaluated by taking a plain source with broadband spectrum in the range from 500-1500 nm and the intensity enhancement is calculated in the range of gaps with the size of $15\,nm \times 15\,nm \times 15\,nm$. Since the metasurface consists of periodically positioned bowtie antennas and the incident wave propagates normal to the surface, we take the periodic boundary conditions along the x- and y-directions. For calculating the reflectance, we put 2D monitor at the edge of calculation domain cut by PML boundary in front of the metasurface and take the result of transmittance through this monitor as the reflectance.

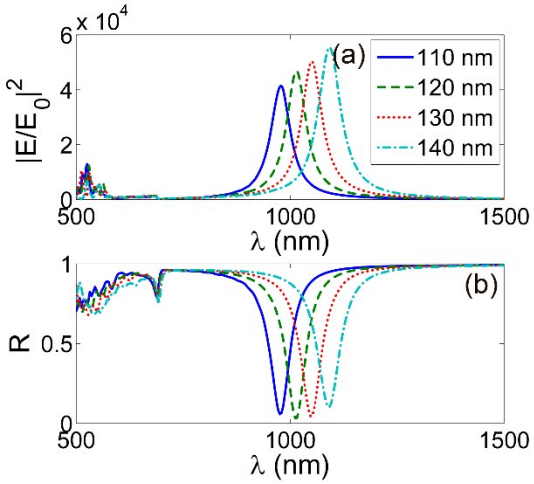

Figure S1. Dependence of maximum intensity enhancement (1a) and reflection (1b) on *h*.

Other structural and material parameters are the same as in Fig. 2.

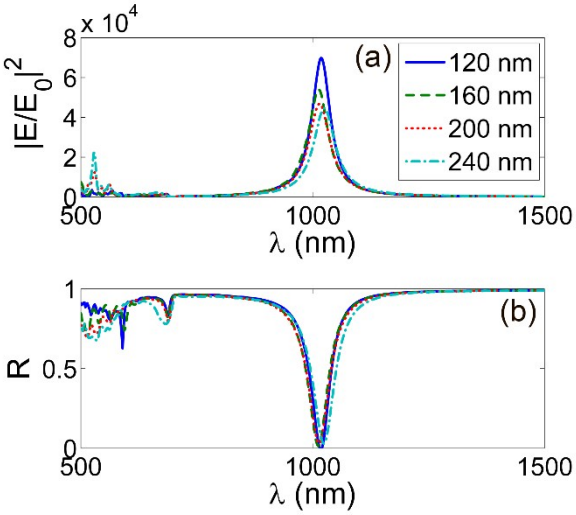

Figure S2. Dependence of maximum intensity enhancement (2a) and reflectance (2b) on *l*. Other structural and material parameters are the same as in Fig. 2.

The structural dependencies of the intensity enhancement and reflectance have been evaluated and presented in Figs. S1 and S2. The figures show that the plasmon resonant wavelength depends mainly on *h*. The magnitude of *l* only affect the intensity enhancement at the resonance.

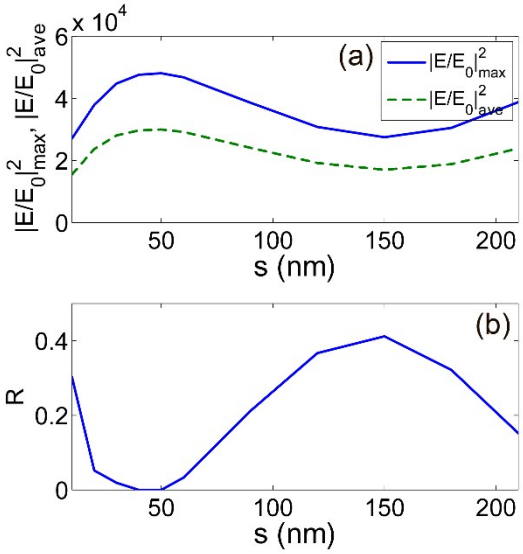

Figure S3. Maximum and averaged intensity enhancements (3a) and reflectance (3b) as the functions of the thickness of silica spacing layer. The other structural and material parameters

of the metasurface are the same as in Fig. 2.

The local field enhancement significantly depends on the thickness *s* of dielectric spacing layer of the reflective substrate as shown in the previous reports (see [S1,S2]). The figure shows that, for the thickness *s* of silica layer from 40 nm to 60 nm, the intensity enhancement reaches the maximum value and the reflectance vanishes.

S2. Numerical details for evaluating second-harmonic generation

As described in the main text, we assume that the optical axis is parallel to the polarization of pump wave. In the case of lithium niobate nonlinear crystal, the total second-order nonlinear polarization can be approximated by $P^{(2)}(2\omega;\omega,\omega) = \chi^{(2)}_{zzz}E^2$, because $\chi^{(2)}_{zzz} = -83.4$ pm/V is an order-of-magnitude larger than the other components of second-order onlinear tensor [S3]. In the above equation for $P^{(2)}(2\omega;\omega,\omega)$, E is the local electric field in LN calculated by FDTD.

In this approximation, we can directly apply built-in tool of Lumerical FDTD for calculating the second-harmonic generation, which considers only the contributions of the diagonal components of $\chi^{(2)}$ tensor. The second-order polarization $P^{(2)}(2\omega;\omega,\omega)$ results in a spectral peak of light reflected from the metasurfaces. For this purpose, the reflectance is obtained from the transmission monitor placed at the interface between the calculation domain and PML region in front of the metasurface. The resultant spectral power of second harmonic is calculated by multiplying the reflectance from the nonlinear metasurface by the source power spectrum.

S3. Numerical evaluation of second-harmonic generation efficiency and comparison with a metasurface consisting of plasmonic rod pair nanoantenna array

S3a. Numerical evaluation of second-harmonic generation efficiency

For calculating the second-harmonic generation efficiency, we use the reflectance (see Supporting Information S1), which is normalized to the peak intensity of pump wave in the frequency domain and display on a logarithmic scale as shown in Fig. 3. Integrating the power spectrum near second-harmonic frequency and calculating its ratio to the total power of pump, we can obtain the resultant conversion efficiency.

S3b. Comparison of second-harmonic generation efficiencies with metasurfaces consisting of rod pair nanoantenna array

Here we present the results of second-harmonic generation from a metasurface made of

plasmonic nanoantenna array of a different shape (nanorod pair antenna, the structure of which is shown in Fig. S4). For comparison, the gap size and the other structural and material parameters are taken to be the same as in Fig. 3.

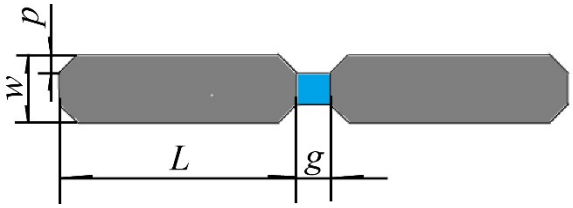

Figure S4. Structure of silver rod pair nanoantennas (gray), the gaps of which are filled with $LiNO_3$ (blue). The metasurface consists of these antenna array and supported by the reflective substrate as in Fig. 1. The other structural and material parameters are the same as in Fig. 2.

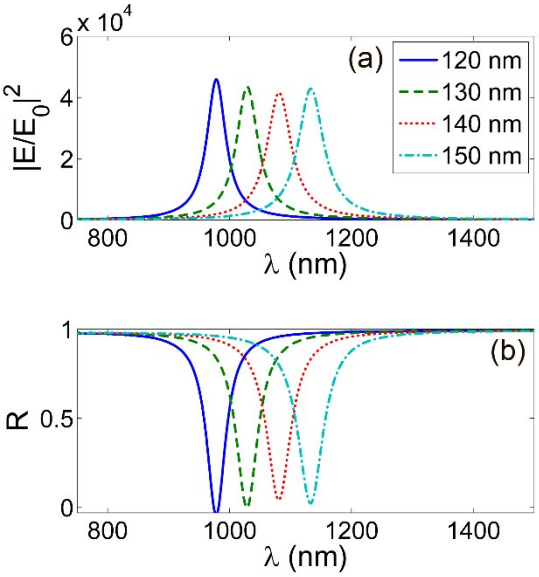

Figure S5. Dependence of maximum intensity enhancement (5a) and reflectance (5b) on nanorod length L. The structural parameters of nanoantenna are as follows: g = 15 nm, p = 30 nm, and w = 15 nm, and other structural and material parameters of the metasurface are the same as in Fig. 2. The incident wave is polarized along the direction of long axis of the nanorods and propagates along the normal to the metasurface.

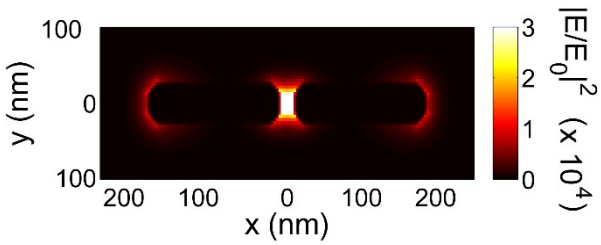

Figure S6. Distribution of intensity enhancement at the mid-height of a nanorod antenna of the metasurface. The length of nanorods is L =130 nm. Other structural and material parameters, the polarization and propagation directions of incident wave are the same as in Fig. S5.

Figures S5 illustrates the dependencies of the intensity enhancement and reflectance on the nanorod length L. The figure shows that the plasmon resonance wavelength red-shifts with increasing L. The distribution of the intensity enhancement at the mid-height of the nanoantenna has been shown in Fig. 6 for a length L = 130 nm of nanorods.

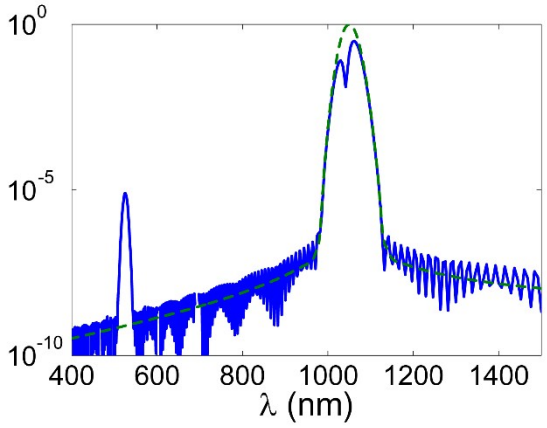

Figure S7. Spectra of pump and second-harmonic waves from the metasurface shown in Fig. S6. Pumping condition is the same as in Fig. 3.: The central wavelength, the duration, and the peak intensity of pump pulse are 1050 nm, 50 fs, and 13.27 MW/cm^2, respectively. The polarization and propagation directions of pump pulse are the same as in Fig. S5.

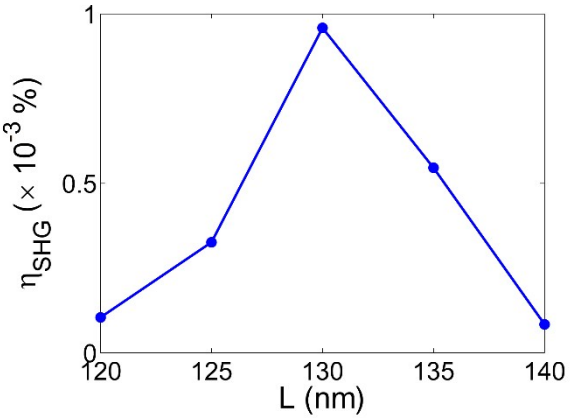

Figure S8. Dependence of second-harmonic generation efficiency η_{SHG} on the nanorod length L. Other structural and material parameters are the same as in Fig. S5. Pumping conditions are the same as in Fig. S7.

Figure S7 shows the spectra of the pump pulse and its second-harmonic component generated from the metasurface of nanorod pair antenna with a length L = 130 nm for the pumping conditions the same as in Fig. 3. The dependence of SHG efficiency η_{SHG} on the length L of nanorods is shown in Fig. S8 for the same peak intensity 13.27 MW/cm^2 of pump. From the figure, one can see that the maximum value of conversion efficiency amounts to about 9.6×10^{-4} %, which is the same as in Fig. S7. The resultant maximum efficiency is two orders-of-magnitude smaller than the case of the metasurface consisting of bowtie silver nanoantenna array (see Figs. 3 and 4), under the same pumping condition.

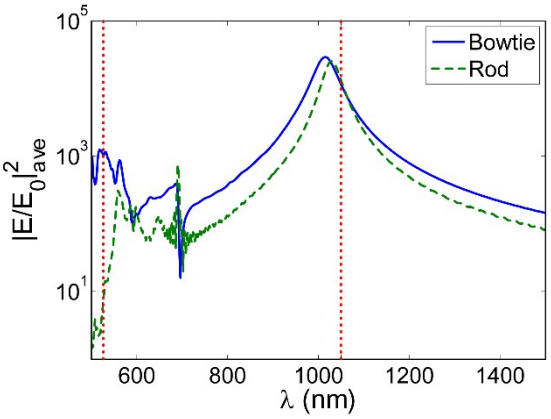

Figure S9. Averaged intensity enhancements $|E/E_0|^2_{ave}$ in metasurfaces consisting of bowtie and rod pair nanoantenna arrays at the wavelengths of fundamental (1050 nm) and second-harmonic waves (525 nm). Averaging is performed in the gap with a volume of $15\ nm \times 15\ nm \times 15\ nm$.

Here we discuss the reason for significantly high conversion efficiency obtained in bowtie antenna array compared with the case of rod pair antennas. Figure S9 shows the intensity enhancement averaged in the volume of gaps filled with lithium niobate. The figure shows that $|E/E_0|^2_{ave}$ has the similar values for both cases, while the bowtie antennas exhibit intensity enhancement about two orders-of-magnitude larger than the nanorod pair antennas. Since the total enhancement of second-order harmonic efficiency is related to the field enhancement $f = E/E_0$ by $g = |f(\omega)|^4 |f(2\omega)|^2$ (see e.g. [S4,S5]), the conversion efficiency depends not only on $f(\omega)$, but the field enhancement $f(2\omega)$ at the second-harmonic frequency as well. From Figure S9, $|f(2\omega)|^2 = |E(2\omega)/E_0(2\omega)|^2$ in the case of bowtie antenna array has the value nearly two orders-of-magnitude larger than the nanorod pair antennas, while the intensity enhancement $|f(\omega)|^2 = |E(\omega)/E_0(\omega)|^2$ at fundamental frequency has the similar magnitudes for both cases. From the above discussions, we can understand why the SHG efficiency from the metasurface of bowtie antenna array is about two orders-of-magnitude higher than the nanorod pair antenna array.

S4. Comparison with metasurfaces supported by silica substrate

Here we present the results for the metasurfaces consisting of bowtie and rod pair antennas supported by silica substrate in comparison with the cases of using silica-coated silver substrates.

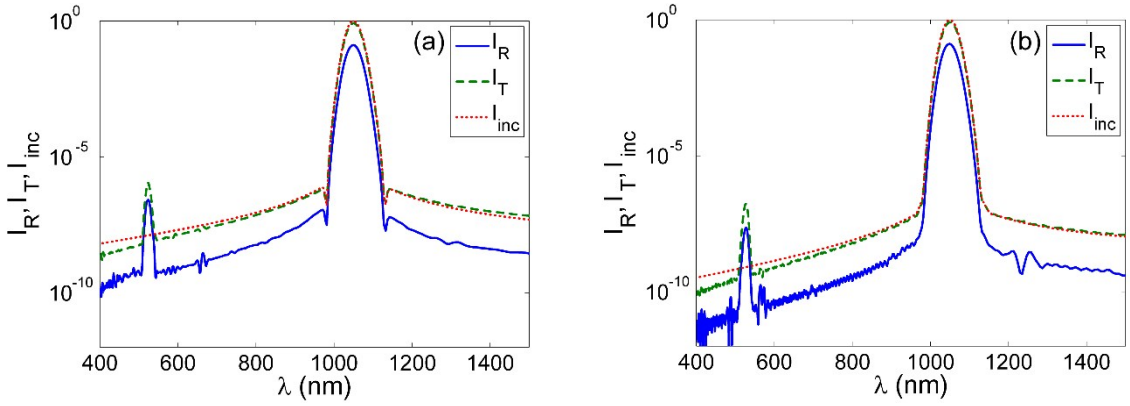

Figure S10. Intensity spectra of reflected (I_R), transmitted (I_T), and pump pulses (I_{inc}) from the metasurfaces consisting of bowtie (a) and rod pair nanoantenna arrays (b). The structural and material parameters are the same as in Figs. 3 (a) and S7 (b), respectively, except that the metasurfaces are supported by silica substrate. The central wavelength, pulse duration, and peak intensity of pump are 1050 nm, 50 fs, and 13.27 MW/cm^2, respectively, as in Figs. 3 and S7.

Figure S10a shows the intensity spectra of the reflected, transmitted, and pump pulses from the metasurface composed of bowtie antenna array supported under pumping condition the same as in Fig. 3, in which all the spectra are normalized to the peak intensity of pump pulse. The only difference of the parameters and structure from Fig. 3 is in the substrate made of only silica. The resultant second-harmonic efficiencies obtained from the reflection and transmission spectra (Fig. S10a) are $\eta_{SHG,R} = 3.64 \times 10^{-5}$ % and $\eta_{SHG,T} = 1.46 \times 10^{-4}$ %, respectively, being 1.48×10^{3} and 3.70×10^{2} times lower than the case of using silica-coated silver substrate, respectively. In Fig. S10b, we have shown the reflection and transmission spectra from the metasurface of rod pair nanoantenna array supported by silica substrate. From the result shown in the figure, we can evaluate the SHG efficiencies for the reflection and transmission to be $\eta_{SHG,R} = 2.82 \times 10^{-6}$ % and $\eta_{SHG,T} = 2.20 \times 10^{-5}$ %, respectively, which are about 340 and 44 times lower than the case of reflective substrate made of silica-coated silver layer shown in Fig. S7. The above results show that we can enhance the SHG efficiency by 2-3 orders-of-magnitude by using reflective substrate compared with the case of transparent dielectric substrates.

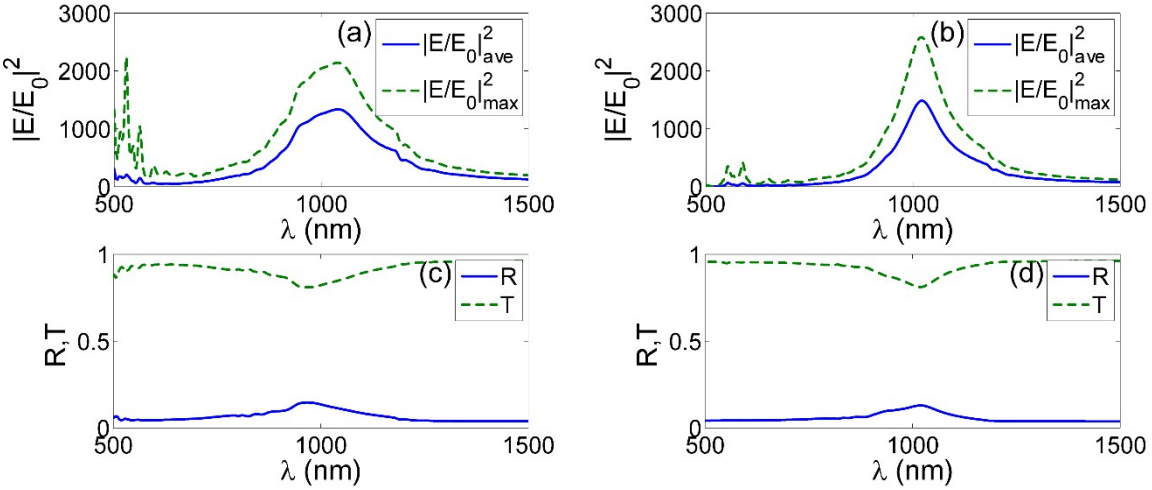

Figure S11. Intensity enhancements $|E/E_0|$^2 and reflection/transmission spectra of metasurfaces composed of bowtie (a, c) and rod pair (b, d) nanoantenna arrays. In c and d, *R* and *T* represent the reflection and transmission coefficients from the metasurfaces, respectively. The structural parameters of metasurfaces shown in S11a and S11b are the same as in Figs. 2 and 3. The structural and material parameters for the results shown in S11 b and d are the same as in Fig. S6 and S7.

Significant enhancement of second-harmonic generation when using the reflective substrates can be understood by evaluating the electromagnetic responses of metasurfaces of plasmonic nanoantenna arrays in comparison with the case of transparent substrate. Figure S11 shows

the intensity enhancement and reflection and transmission spectra in the linear case for both bowtie (Figs. S11a and S11c) and rod-pair nanoantenna arrays (Figs. S11b and S11d), respectively. The only difference from Figs. 2 and S5 (green dashed lines) is in the substrate is made of only silica. The figure shows that the wavelength at which the local intensity resonantly enhances is not significantly changed for both cases, while the spectral width becomes much wider and, especially, the field enhancement is significantly lower than the case of using reflective substrate, leading to the severely reduced conversion efficiency.
The above results clearly prove the reason for the remarkably high SHG efficiency from the metasurfaces supported by reflective substrates.

S5. Dependence of intensity enhancement and reflectance on structural parameters in metasurface consisting of bowtie silver nanoantenna surrounded by argon gas

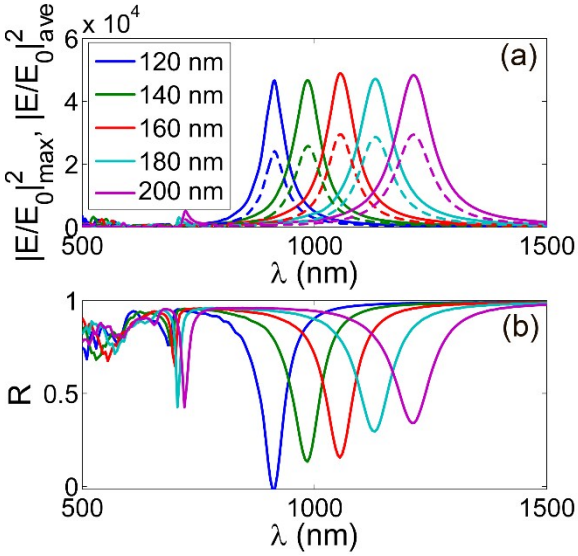

Figure S12. Intensity enhancement and reflectance in metasurface consisting of bowtie silver nanoantenna array for different values of h (Fig. 6a). The metasurface is supported by a reflective silica-coated silver substrate and surrounded by argon gas. In a, solid lines present the maximum $|E/E_0|^2_{max}$ intensity enhancements and dashed lines the averaged $|E/E_0|^2_{ave}$, respectively, where averaging is performed over the volume of $15\ nm \times 15\ nm \times 15\ nm$ in the gap region. Other structural and material parameters are the same as in Fig. 6b.

S6. Lewenstein model for high-harmonic generation in noble gas near the plasmonic nanostructures

High harmonics are generated through the following steps: tunneling ionization due to pumping with strong laser pulse, the acceleration of free electron generated by the ionization and returning to the nucleus by the oscillating electric field of pump, and the emission of high

harmonics upon recombination of the electron with the parent ion. The above processes are described well by Lewenstein model (see e.g. [S6-S8]). In this model [S9,S10], the contributions of all bound states are neglected except the ground state and electrons in the continuum are considered as free particles moving in the electric field of pumping light without effect of Coulomb potential. The ponderomotive energy U_p possessed by ionized electron is assumed to be much smaller than saturation energy, thus the depletion of ground state is neglected [S9]. The ionization energy I_p should be much larger than unity (typically $I_p \approx 5-20$ photons of pump) and U_p is comparable or larger than I_p [S9]. In the case of argon gas pumped at 1050 nm, for example, the ionization energy $I_p = 15.76$ eV is about 13.35 times larger than the photon energy. The above approximations are valid when noble gases are used for high-harmonic generation under pumping with peak intensity of 10^{14}-10^{15} W/cm^2 [S9].
In the Lewenstein's strong field model, the induced dipole moment contributing to the high-harmonic generation can be described by [S11]

$$x(t) = i\int_0^{\infty}\left(\frac{\pi}{\varepsilon + i\tau/2}\right)^{1.5} d_x^*\left[p_{st}(t,\tau) - A(t)\right] d_x\left[p_{st}(t,\tau) - A(t-\tau)\right], \\ \times E_{enh}(t-\tau)\exp\left[-iS_{st}(t,\tau)\right]d\tau + c.c.$$

where $p_{st}(t,\tau) = \tau^{-1}\int_{t-\tau}^{t} A(t')dt'$ is the classical action, $S_{st}(t,\tau) = \left(I_p - \frac{1}{2}p_{st}^2\right)\tau + \frac{1}{2}\int_{t-\tau}^{t} A^2(t')dt'$, A is the vector potential for the plasmon-enhanced local field E_{enh}, and I_p is the ionization energy of the atom. Here all the expressions are described in the atomic unit. For hydrogen-like atoms, the dipole matrix element is described by $d_x(p) = i2^{3.5}\alpha^{1.25}\pi^{-1}p/(p^2+\alpha)$, where α is taken to be $2I_p$. The high-harmonic generation efficiency is calculated by using the formula $\eta(N_{HH}) = \omega^4 N_{HH} T\left(12\pi\varepsilon_0 c^3\right)^{-1}\int |x(\omega)|^2 dV/\Phi$ [S11], where V is the volume of the space occupied by the high-harmonic dipoles, $N_{HH} = \omega/\omega_0$ is the harmonic order, ω and ω_0 are the angular frequencies of high-harmonic and fundamental waves, T is the time window for which Fourier transform is performed, Φ is the energy of pump pulse, ε_0 is the permittivity of vacuum, c is the light velocity in vacuum, respectively.

References

[S1] T. J. Seok, A. Jamshidi, M. Kim, S. Dhuey, A. Lakhani, H. Choo, P. J. Schuck, S. Cabrini, A. M. Schwartzberg, J. Bokor, E. Yablonovitch, M. C. Wu, Radiation Engineering of Optical Antennas for Maximum Field Enhancement, *Nano Lett.* **11**, 2606-2610 (2011).
[S2] X. Zhu, H. Shi, S. Zhang, Q. Liu, H. Duan, Constructive-interference-enhanced Fano resonance of silver plasmonic heptamers with a substrate mirror: a numerical study, *Opt.*

Express **25**, 9938-9946 (2017).
[S3] D. N. Nikogosyan, *Nonlinear Optical Crystals: A Complete Survey*, Springer, New York, 2005.
[S4] N. Weber, M. Protte, F. Walter, P. Georgi, T. Zentgraf, C. Meier, Double resonant plasmonic nanoantennas for efficient second harmonic generation in zinc oxide, *Phys. Rev. B* **95**, 205307 (2017).
[S5] K.-Y. Yang, J. Butet, C. Yan, G. D. Bernasconi, O. J. F. Martin, Enhancement mechanisms of the second harmonic generation from double resonant aluminum nanostructures, *ACS Photonics* **4**, 1522-1530 (2017).
[S6] I. J. Kim, C. M. Kim, H. T. Kim, G. H. Lee, Y. S. Lee, I. Y. Park, Highly efficient high-harmonic generation in an orthogonally polarized two-color laser field, *Phys. Rev. Lett.* **94**, 243901 (2005).
[S7] A. T. Le, X.-M. Tong, C. D. Lin, Evidence of two-color interference in high-order harmonic generation from CO_2, *Phys. Rev. A* **73**, 041402 (2006).
[S8] X. Zou, R. Lock, N. Wagner, W. Li, H. C. Kapteyn, M. M. Murnane, Elliptically polarized high-order emission from molecules in linearly polarized laser fields, *Phys. Rev. Lett.* **102**, 073902 (2009).
[S9] M. Lewenstein, P. Balcou, M. Y. Ivanov, A. L'Huiller, P. B. Corkum, Theory of high-harmonic generation by low-frequency laser fields, *Phys. Rev. A* **49**, 2117-2132 (1994).
[S10] M. Lewenstein, A. L'Huiller, Principles of single atom physics: High-order harmonic generation, above-threshold ionization and non-sequential ionization, in *Strong Field Laser Physics*, T. Brabec ed., Springer, New York, 2008.
[S11] K.-H. Kim, A. Husakou, J. Herrmann, High-order harmonic generation employing field enhancement by metallic fractal rough surfaces, *Opt. Express* **19**, 20910-20915 (2011).